Automodulations in Kerr-lens mode-locked solid-state lasers

J. Jasapara and W. Rudolph

Department of Physics and Astronomy, University of New Mexico, Albuquerque, New Mexico 87131

V. L. Kalashnikov, D. O. Krimer and I. G. Poloyko

International Laser Center, 65 Skorina Avenue, Building 17, Minsk 220027, Belarus

M. Lenzner

Department of Quantum Electronics and Laser Technology, Vienna University of Technology, A-1040 Vienna, Austria

Received May 27, 1999; revised manuscript received September 27, 1999

Nonstationary pulse regimes associated with self-modulation of a Kerr-lens mode-locked Ti:sapphire laser have been studied experimentally and theoretically. Such laser regimes occur at an intracavity group delay dispersion that is smaller than or larger than what is required for stable mode locking and exhibit modulation in pulse amplitude and spectra at frequencies of several hundred kilohertz. Stabilization of such modulations, leading to an increase in the pulse peak power by a factor of 10, were accomplished by weak modulation of the pump laser with the self-modulation frequency. The main experimental observations can be explained with a round-trip model of the femtosecond laser, taking into account gain saturation, Kerr lensing, and second- and third-order dispersion. © 2000 Optical Society of America [S0740-3224(00)01502-2]

OCIS codes: 320.5550, 320.7090, 320.7160, 270.5530.

1. INTRODUCTION

Nonstationary regimes of ultrashort-pulse generation in lasers have gained a great deal of attention in recent years. Whereas the stable operation of femtosecond lasers is usually the preferred mode of operation, nonstationary regimes provide unique opportunities to explore the physical mechanisms that lead to the formation and stabilization of ultrashort pulses. The trend toward generating ever shorter pulses from laser oscillators makes it desirable to characterize the parameter range of stable operation in detail. This includes the boundaries of such regimes and the processes leading to nonstationary pulse behavior. However, self-modulation or induced modulation of such lasers can increase the peak power at a reduced repetition rate and are thus attractive for pulse amplification or in experiments in which oscillators do not provide sufficient pulse energies.

Various self-starting and induced nonstationary pulse modes in femtosecond dye and in solid-state lasers have been reported, among them cavity dumping,[1] higher-order soliton formation,[2,3] and periodic amplitude modulations.[4] In recent years several kinds of periodic pulse amplitude modulation have been observed in Ti:sapphire lasers after insertion of apertures or adjustment of the dispersion.[5] Also, cavity dumping[6] and oscillations between transverse modes[7,8] have been realized successfully in Ti:sapphire lasers. In this paper we describe experiments and theoretical results of automodulations in femtosecond Ti:sapphire lasers that occur with frequencies typical for relaxation oscillations.

There are two major approaches to describe the complexity of femtosecond lasers—the round-trip model, in which the pulse passes through discrete elements, and the continuous model, in which the action of individual laser components is distributed uniformly in an infinitely extended hypothetical material.[9] Both models allow for analytical as well as numerical approaches. The most successful round-trip model was developed more than 20 years ago[10] and relied on the expansion of the transfer functions of the individual laser elements. It yielded an analytical sech solution for the pulse envelope. Later this model was extended to include self-phase modulation (SPM) and dispersion leading to sech pulse envelopes and tanh phases.[11] In a stationary regime the pulses reproduce after one or several round trips and thus exhibit features of solitary waves and solitons.

In femtosecond Ti:sapphire lasers the major pulse-shaping mechanisms are Kerr lensing, SPM, and group delay dispersion (GDD). A large number of theoretical approaches exist to describe various features of such lasers.[12–16] The main condition for pulse stability against the buildup of noise (spontaneous emission) is the negative net gain outside the pulse. Whereas in femtosecond dye lasers this is realized by the interplay of a slow saturable absorber and gain saturation, in Kerr-lens mode-locked (KLM) solid-state lasers a fast saturable absorber effect that is due to Kerr lensing provides the positive gain window. Outside the parameter range for stable pulses, periodic and stochastic pulse modulations have been predicted.[17] Our theoretical approach in this

paper is based on a modified round-trip model[18] and tracks the changes of amplitude and phase parameters of the pulse from one round trip to the next. As we shall see, the inclusion of cavity third-order dispersion is crucial to describing the nonstationary pulse modes.

In the first part of the paper we describe two different self-modulation modes observed at GDD greater than and smaller than what is required for stable mode locking. In the second part we present a theoretical model based on a stability analysis of the Kerr-lens mode locking that explains the main experimental findings.

2. EXPERIMENT

A soft-aperture KLM Ti:sapphire laser was set up in the usual four-mirror configuration with a 3-mm-thick crystal between two focusing mirrors of 5-cm focal length, two fused-silica prisms for dispersion compensation, and a 5% outcoupling mirror. It was pumped with 4.5 W, all lines of an argon-ion laser. The two distinctly different regimes of self-modulation A (B) were realized by means of increasing (decreasing) the insertion of one of the compensating prisms, that is, by addition (subtraction) of positive GDD starting from stable mode locking.

To obtain regime A, the intracavity prism insertion (glass path) is increased. The spectrum first broadens and blue shifts until it exhibits a maximum at ~730 nm with a tail extending out to 900 nm. At this point, spikes develop at the short- and the long-wavelength ends of the spectrum. A further increase in the intracavity glass path beyond this point destroys the mode locking. A perturbation of the cavity (e.g., pushing one of the end mirrors or rocking one of the prisms) results in a modulation of the pulse train of the Ti:sapphire laser, which can be stabilized when the prism is pulled out slightly and gradually. The resulting pulse train and spectrum are shown in Figs. 1(a) (upper curve) and 1(b). This modulation is similar to the self-*Q*-switching observed in Ref. 5. Although the cavity *Q* is not switched in a strict sense and the modulations rather resemble relaxation oscillations, we will keep the term self-*Q*-switching. The peak amplitude under the *Q*-switch envelope is approximately ten times higher than the amplitude in the cw mode-locked regime. As can be seen from the figure, the self-*Q*-switch period is ~5 μs, and the width of the *Q*-switch envelope is ~1 μs. The *Q*-switched pulses are separated by prelasing regions. The average pulse duration without external pulse compression was measured to be ~130 fs (after 6 mm of fused silica). We compared the second harmonic of the pulse train with the square of the fundamental signal. From that the pulse duration seemed to be constant over the *Q*-switched pulse and the prelasing region. Information on the spectral evolution across the *Q*-switched pulse was gained by means of recording the output of a fast photodiode placed at the exit slit of a monochromator (bandwidth 1.5 nm). The results shown in Fig. 2 indicate that the spectrum of the pulses under the *Q*-switched envelope evolves with time on either side of the central wavelength.

We observed a second self-modulation mode, B, when the cavity prism was translated so as to decrease the intracavity glass path, that is, to increase the negative GDD

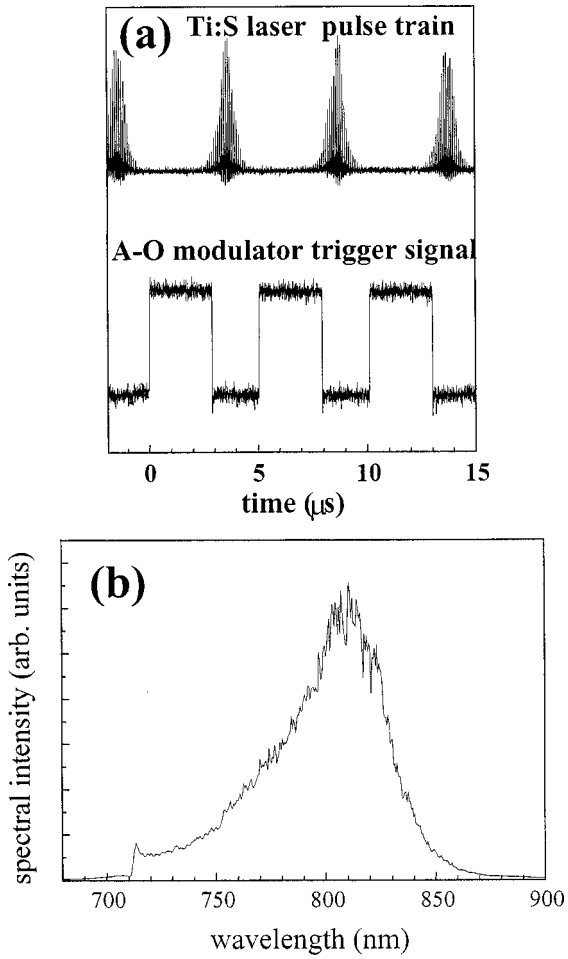

Fig. 1. (a) Pulse train from a mode-locked Ti:sapphire laser in self-*Q*-switched regime A (upper curve) and the acousto-optic (A-O) driver signal used when the pump laser was modulated. On the time scale shown here there was no observable difference between the Ti:sapphire laser pulse train with the modulated and the unmodulated pump laser. (b) Laser spectrum observed during regime A. The fluctuations in the pulse train resulted from an inadequate sampling rate of the digital oscilloscope (512 sampling points during the 17-μs time window).

of the laser cavity. During translation of the prism, the spectrum moved toward longer wavelengths and began to narrow until, at one point, the laser jumped into a strongly self-modulated mode-locked regime of operation. The modulated pulse train and pulse spectrum are shown in Figs. 3(a) and 3(b), respectively. Again, no measurable variation of the pulse duration over the modulation period and the prelasing region was observed. The pulse duration was ~40 fs (after ~6 mm of fused silica). We also monitored the modulated pulse train through a monochromator. We found strong modulations in the spectral intensity at various wavelengths across the duration of the modulated envelope; some examples are shown in Fig. 4. The spectrum [cf. Fig. 3(b)] and the spectral modulations (cf. Fig. 4) across the envelope bear close resemblance to the observation of higher-order solitons reported in Refs. 2 and 3.

Phenomenologically, the existence of regime A can be explained by relaxation oscillations and by the interplay of SPM and GDD in the laser. Mode A arises when ex-

cess glass is inserted into the cavity, that is, introducing positive GDD. According to the soliton model of the laser, a balance of positive chirp due to SPM and negative chirp due to GDD can result in a steady-state pulse regime. The prism insertion introduces positive GDD that leaves part of the positive chirp due to SPM uncompensated. SPM is proportional to the product of nonlinear refractive index and pulse intensity and is thus dependent on the quotient of pulse energy and duration. Hence, with excess glass, pulses of lower energy but equal pulse duration can still be supported. These low-energy pulses make up the observed prelasing regime. Because of this low-intensity lasing, the inversion begins to build up in the gain medium until dumped into the *Q*-switched pulse. The modulation is driven by relaxation oscillations. In the leading edge of the *Q*-switched pulse the intensity of the mode-locked pulses begins to increase while its duration remains constant. As a result of the higher intensity the SPM begins to generate new spectral components as indicated by the spectral broadening seen later in the *Q*-switched envelope.

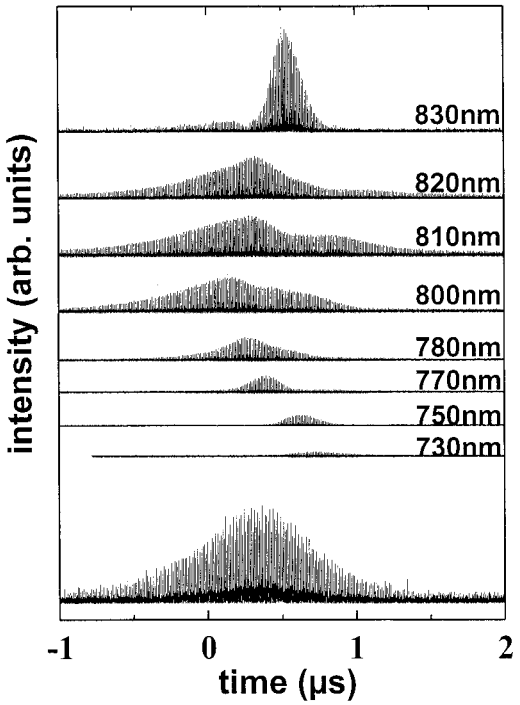

Fig. 2. Temporal position of the various spectral components relative to the peak of the *Q*-switched envelope (bottom curve).

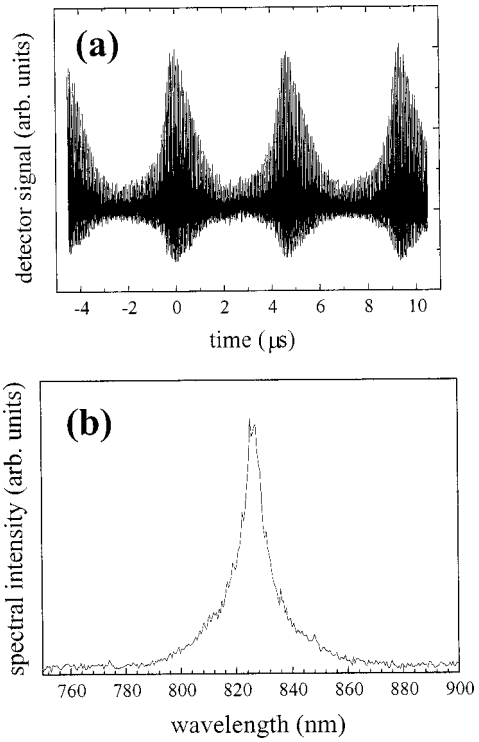

Fig. 3. (a) Pulse train and (b) spectrum observed in regime B.

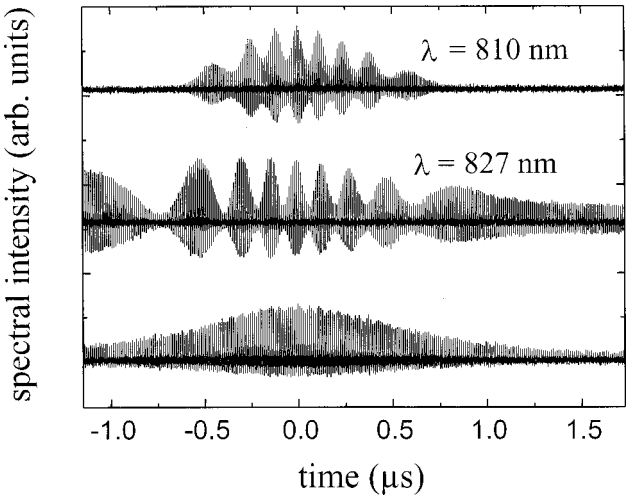

Fig. 4. Temporal behavior of spectral components at 810 and 827 nm in regime B and the mode-locked pulse train (bottom curve).

Both modulation regimes A and B were subject to random fluctuations in pulse length, height, and repetition frequency. To stabilize operational mode A, we modulated the pump laser (modulation depth, ~5%), using an acousto-optic modulator. The modulator was driven by the amplified output of a photodiode that monitored the pulse train of the Ti:sapphire laser. Figure 1(a) shows the *Q*-switched pulse train and the trigger signal for the modulator. It was also possible to force modulation with an external oscillator tuned to near the free-running *Q*-switch frequency of ~200 kHz. The more than tenfold increase in the pulse energy in the peak of the *Q*-switched pulse (≅30 nJ) as compared with the ordinary mode locking makes this mode of operation attractive for subsequent high-repetition-rate pulse amplifiers and for applications that require a higher energy than what is available from oscillators.

3. THEORY

Our aim in this section is to discuss some general aspects of pulse regimes with periodic modulation and then focus on cases that describe our experimental observations, in particular, regime A. To this end we proceed in two steps: first, only the second-order GDD is taken into account, and second, we will add a third-order dispersion term.

Assuming that the change of the pulse envelope during one round trip is small, the laser dynamics can be described by a nonlinear equation of the Landau–Ginzburg type[10,19]:

$$\frac{\partial a(k,t)}{\partial k} = \left[\alpha - l + (1 + id)\frac{\partial^2}{\partial t^2} + (\sigma - i\beta)|a|^2\right]a(k,t). \tag{1}$$

Here $a(k,t)$ is the electric field amplitude; k is the round-trip number; t is the local time normalized to the inverse gain bandwidth t_g, which for Ti:sapphire is $\sim$2.5 fs; α is the saturated gain coefficient; l is the linear loss; and d is the GDD coefficient normalized to ${t_g}^2$. The factor before the second derivative, $(1 + id)$, takes into account GDD and the bandwidth-limiting effect of the cavity. For the latter we assume that the bandwidth of the gain medium plays the dominant role. The final summand consists of two parts, a fast absorber (Kerr-lensing) term $\sigma|a|^2$ and a SPM term $-i\beta|a|^2$. For both terms we assumed saturating behavior according to $\sigma = \sigma_0(1 - {}^1\!/_2\,\sigma_0|a_0|^2)$ and $\beta = \beta_0(1 - {}^1\!/_2\,\beta_0|a_0|^2)$, respectively. Here a_0 is the pulse peak amplitude and $\beta_0 = (2\pi L n_2/\lambda n)$ is the unsaturated SPM coefficient for the Ti:sapphire crystal with $n_2 = 1.3 \times 10^{-16}\,\mathrm{cm^2/W}$ and $n = 1.76$ being the nonlinear and the linear refractive indices, respectively. $L = 3$ mm is the length of the crystal, and $\lambda = 800$ nm is the laser center wavelength. Throughout the paper both $|a_0|^2$ and $|a|^2$ are normalized to $5.9 \times 10^{11}\,\mathrm{W/cm^2}$ and β_0 and σ_0 to $1.7 \times 10^{-12}\,\mathrm{cm^2/W}$.

The magnitude of σ_0 can be controlled by the cavity alignment and for typical KLM lasers σ_0 is $10^{-10} - 10^{-13}\,\mathrm{cm^2/W}$.[20] The saturation behavior of both β and σ was introduced phenomenologically to avoid nonphysical solutions at high pulse intensities and is used to describe various complicated processes that, among other things, depend on focusing and on the resonator geometry and alignment. The saturation of SPM is due, for example, to the next-higher-order term in the expansion for the refractive index, the n_4 term. The approximation that the saturation term depends on the peak intensity rather than on the instantaneous intensity is necessary for solving Eq. (1) analytically. In the calculation we vary both σ_0 and β_0 to analyze regimes with different relative strength of amplitude and phase-modulation effects.

The gain coefficient α, during one round trip, changes, owing to depopulation by the laser pulse, gain relaxation with a characteristic time T_{31} ($\approx$3 μs for Ti:sapphire), and the pumping process:

$$(\mathrm{d}\alpha/\mathrm{d}t) = \sigma_{14}(\alpha_m - \alpha)I_p/h\nu_p - \sigma_{32}\alpha|a|^2/h\nu - \alpha/T_{31}. \tag{2a}$$

Here $\sigma_{14} = 10^{-19}\,\mathrm{cm^2}$ and $\sigma_{32} = 3 \times 10^{-19}\,\mathrm{cm^2}$ are the absorption cross section and the emission cross section of the active medium, respectively; α_m is the unsaturated gain coefficient; ν_p and ν are the pump frequency and the laser frequency, respectively; and I_p is the pump intensity. From this equation of the gain evolution one can derive a relation between the gain after the $(k + 1)$th round trip (left-hand side of the equation, primed quantity) and the kth round trip (right-hand side of the equation):

$$\alpha' = \alpha\exp\left(-2\tau|a|^2t_p - \frac{T_{\mathrm{cav}}}{T_{31}} - U\right) + \frac{\alpha_m U}{(U + T_{\mathrm{cav}}/T_{31})}\left[1 - \exp\left(-\frac{T_{\mathrm{cav}}}{T_{31}} - U\right)\right], \tag{2b}$$

where t_p is the laser pulse duration normalized to t_g and T_{cav} ($\approx$10 ns) is the cavity round-trip time. The quantity τ^{-1} is the gain saturation fluence ${E_g}^s$($\approx$0.82 J/cm^2) normalized to $(\lambda n t_g/2\pi z n_2)$ ($\approx 1.5 \times 10^{-3}\,\mathrm{J/cm^2}$) for which we obtain a value of 555 that was used in our calculations. $U = (\sigma_{14}T_{\mathrm{cav}}/h\nu_p)I_p$ is a dimensionless pump parameter, which we chose close to 4×10^{-4} (for a pump beam waist of 50 μm this corresponds to $\sim$4-W pump power). When we analyze stationary regimes where the pulses reproduce after each round trip, a steady-state gain coefficient is used that can be obtained when we set $\alpha = \alpha'$ in Eq. (2b). In the simulation of nonstationary regimes (for example, automodulations) the gain coefficient α changes from round trip to round trip as described by Eq. (2b).

As is known (see, for example, Ref. 12), Eq. (1) has a quasi-soliton solution of the form

$$a(k,t) = a_0\,\mathrm{sech}^{1+i\psi}(t/t_p)\exp(i\phi k), \tag{3}$$

where ψ is the chirp term and ϕ is the constant phase accumulated in one cavity round trip. To investigate the pulse stability, we used a so-called aberrationless approximation,[21] which allows us to investigate the dependence of the pulse parameters on the round-trip number k. After substituting the ansatz (3) into Eq. (1) and expanding all terms with respect to t up to the third order, we obtain three ordinary differential equations with respect to k. The solution of this system by the forward Euler method relates the unknown pulse duration t_p, chirp parameter ψ, and peak amplitude a_0 after the $(k + 1)$th round trip (left-hand side of the equations, primed quantities) to the pulse parameters after the kth transit (right-hand side of the equations):

$$t_p' = t_p + \frac{4 - 7d\psi - 3\psi^2 + (\phi\psi - 2\sigma{a_0}^2 - \psi\beta{a_0}^2){t_p}^2}{2{t_p}^2}, \tag{4a}$$

$$\psi' = (1 - 2\sigma{a_0}^2)\psi + (\phi - \beta{a_0}^2)\psi^2 + \phi - 3\beta{a_0}^2 - \frac{5d + 3\psi + 5d\psi^2 + 3\psi^3}{{t_p}^2}, \tag{4b}$$

$$a_0' = a_0\left[1 + \frac{d\psi - 1 + (\alpha - l - \sigma{a_0}^2){t_p}^2}{{t_p}^2}\right]. \tag{4c}$$

A fourth equation yields the phase delay,

$$\phi = \beta{a_0}^2 + \frac{d + \psi}{{t_p}^2}. \tag{4d}$$

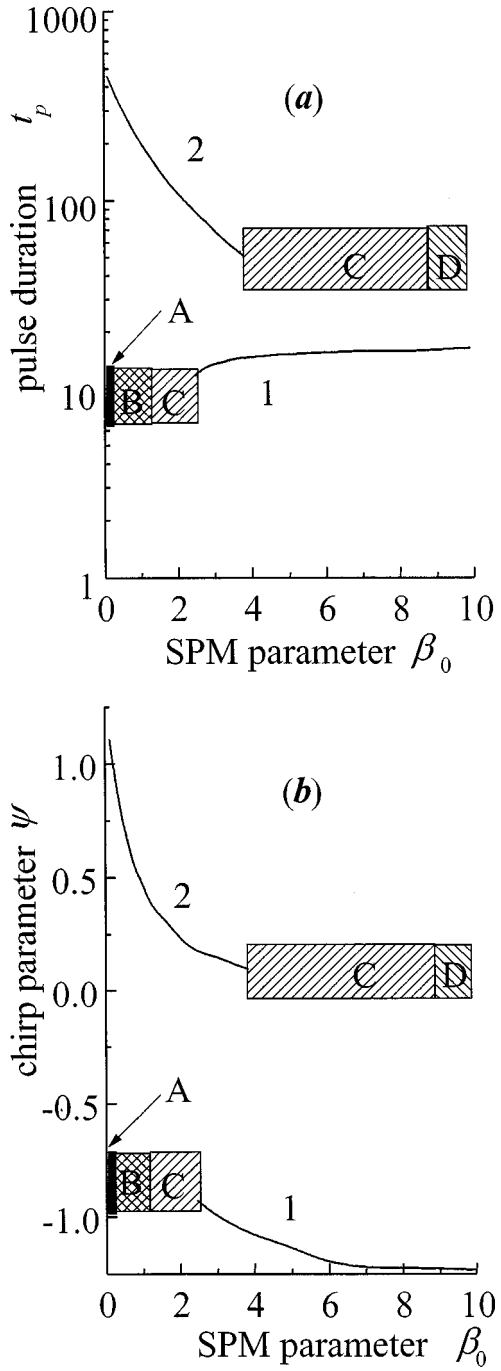

Fig. 5. Steady-state pulse duration (a) and chirp (b) versus the normalized SPM coefficient β_0 for a normalized GDD coefficient of $d = 0$ (curve 1) and $d = -10$ (curve 2). The other laser parameters are $\sigma_0 = 1$, $l = 0.05$, $\alpha_m = 0.5$, $U = 4 \times 10^{-4}$, $L = 0.3$ cm, $\lambda = 800$ nm, and $T_{cav} = 10$ ns. The hatched regions describe various nonstationary pulse regimes (see text).

Equations (4a)–(4c) describe a stationary pulse regime if the complex pulse envelope reproduces itself after one cavity round trip; that is, the pulse parameters to the left- and the right-hand sides of the equal to sign are identical. Within a certain range of laser parameters such a stationary regime usually develops after a few thousand round trips, and the stationary pulse parameters can be obtained by solution of the system of algebraic equations. In an unstable or periodically modulated pulse regime the evolution of the pulses can be followed by calculation of the new pulse parameters after one additional round trip and by use of these results in the right-hand side of Eqs. (4a)–(4d), i.e., as input for the next round trip.

We first study the behavior of the laser when the SPM parameter β_0 and the self-amplitude parameter σ_0 are varied. Physically this can be accomplished when we change the focusing into the crystal and change the cavity alignment or when we insert intracavity apertures, respectively.

Figures 5–7 summarize our evaluation of the mode

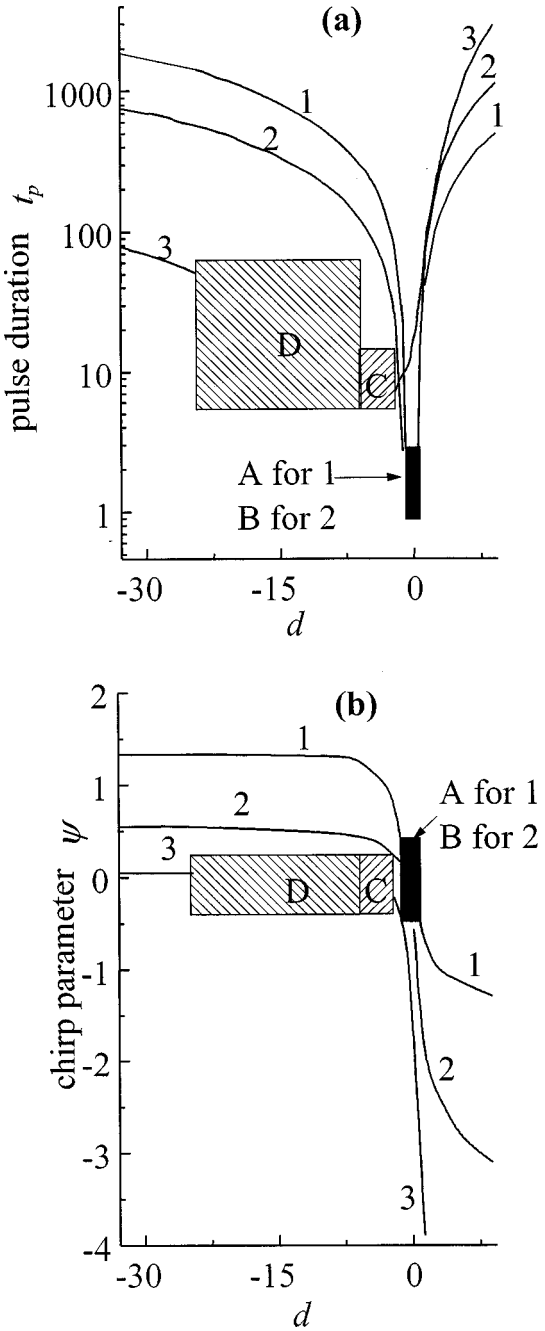

Fig. 6. Steady-state pulse duration (a) and chirp (b) versus the normalized GDD coefficient d for $\beta_0 = 1$ and $\sigma_0 = 10$ (curve 1), $\sigma_0 = 1$ (curve 2), $\sigma_0 = 0.1$ (curve 3). The other parameters are the same as in Fig. 5.

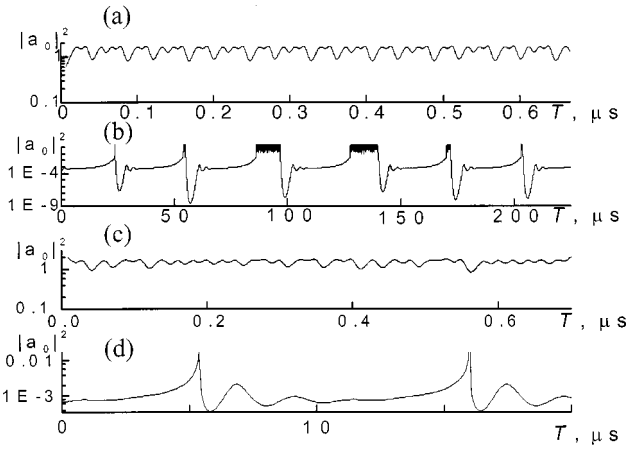

Fig. 7. Normalized pulse intensity $|a_0|^2$ (log scale) versus global time T. The laser parameters for the different curves are chosen as follows: Curve a: $U = 4 \times 10^{-4}$, $\beta_0 = 0$, $d = 0$; $\sigma_0 = 1$. Curve b: $U = 5 \times 10^{-4}$, $\beta_0 = 0$, $d = -10$; $\sigma_0 = 1$. Curve c: $U = 4 \times 10^{-4}$, $\beta_0 = 1$, $d = 0$; $\sigma_0 = 1$. Curve d: $U = 6 \times 10^{-4}$, $\beta_0 = 1$, $d = -20$; $\sigma_0 = 0.1$.

locking based on Eqs. (4a)–(4d). Figures 5 and 6 show pulse duration and chirp as a function of the SPM parameter β_0 and the GDD parameter d, respectively. The solid curves describe steady-state regimes where the pulse parameters reproduce themselves after one round trip, and the rectangles indicate various unstable or periodic pulse modes. Note that these areas refer to a certain part of a curve rather than to a two-dimensional parameter range. In region A regular (periodic) oscillations of the pulse parameters occur, whereas in region B these oscillations are irregular. Region C denotes the parameter range where there is no solution to Eq. (1) in the form of ansatz (3). Region D describes oscillations that have a quasi-regular character. Figure 7 depicts the normalized pulse intensity versus the global time $T = T_{\mathrm{cav}} k$.

Curve 1 of Fig. 5 describes the (hypothetical) situation of zero GDD. For small SPM, $\beta_0 < 0.016$ (region A), the pulse regime is unstable. A closer inspection [see Fig. 7(a)] reveals regular oscillations of the pulse amplitude in this parameter range. The Fourier spectrum of these oscillations shows seven peaks that broaden rapidly if the pump power is increased. The resulting broad frequency spectrum indicates a chaotic behavior of the pulse parameters. An example of the strong dependence of the amplitude modulation on the pump power is illustrated in Fig. 7, curves a and b. A further increase of the SPM, $0.016 < \beta_0 < 1.3$ (region B), leads to irregular oscillations of the pulse parameters, as can be seen in Fig. 7(c). Even larger SPM, $\beta_0 > 2.6$, results in stable pulses. Only Fig. 7(d) describes a regime that refers to the experimental section. The other curves are more of theoretical interest, because they treat situations in which the pulse parameters become unstable.

Curve 2 in Fig. 5 is in the presence of GDD. A comparison with curve 1 shows that GDD stabilizes the pulse generation in the region of small β_0, $\beta_0 < 3.9$, however, at substantially longer pulses. We find the stabilization to be due mainly to a smaller effect of nonlinearities as a result of the longer pulse duration and the subsequently lower intensities. In all cases depicted in Figs. 5 and 6, approaching regions of instability means increasing the pulse energy. This leads to stronger gain saturation, which makes the onset of relaxation-oscillation-driven instabilities more likely.

Figure 6 depicts pulse duration and chirp as a function of the GDD parameter d for a constant SPM parameter $\beta_0 = 1$ and different σ_0, that is, different magnitude of the amplitude modulation term. Stable pulses over a broad range of the GDD can be expected for larger values of σ_0 (curves 1 and 2). There is no stable regime near zero GDD (solid rectangle). For small values of σ_0 (curve 3) there is a broad range of unstable pulse behavior (area D). Stable pulses occur at large negative GDD and near zero and positive GDD. Except for a region near zero GDD, a larger σ_0 results in longer pulses.

In summary, two distinctly different stable pulse modes exist. The first mode results in strongly chirped output pulses [Fig. 5(b)] of short (cf. Fig. 5, curve 1) or long duration (cf. Fig. 5, curve 2) depending on whether the effective phase nonlinearity β_0 is large or small. In these regimes any pulse shortening due to the fast absorber action and any spectral broadening due to SPM are counteracted by the bandwidth-limiting element. The second mode shows the features of solitary pulse shaping; that is, the interplay of GDD and SPM nonlinearities results in a quasi-Schrödinger soliton pulse with small chirp [cf. Fig. 6(b), curve 3 to the left-hand side of region D]. The pulse area agrees with what is predicted from the nonlinear Schrödinger equation for a fundamental soliton.

At small σ_0 (curve 3, Fig. 6), decreasing the amount of negative GDD from the stable pulse regime results in periodic oscillations of the pulse intensity (region D). This behavior describes our experimental observations (cf. Figs. 1 and 2). The calculated temporal evolution of the pulse amplitude is detailed in Fig. 7(d). The Q-switch pe-

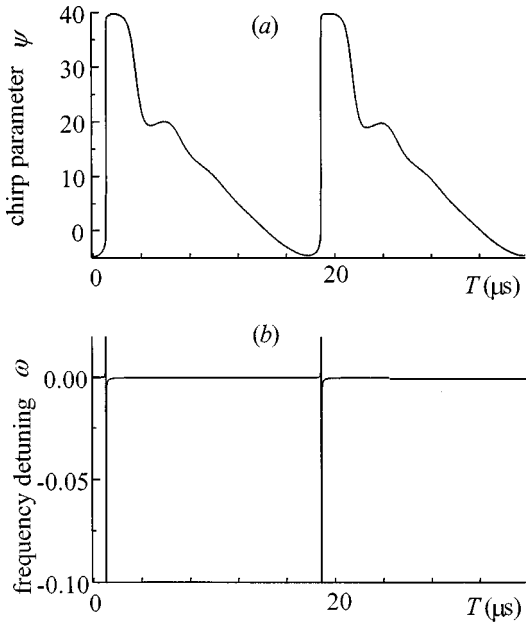

Fig. 8. Pulse chirp ψ (a) and normalized frequency shift ω (b) versus global time T for the laser parameters used in Fig. 7, curve d, and $d_3 = -30$.

riod is close to the gain relaxation time T_{31}, a fact that supports the notion that this behavior is driven by relaxation oscillations.

The experimental observations were made near zero GDD where higher-order dispersion effects are more likely to play a role. Therefore, in the next step, we included a third-order dispersion term in our model; i.e., we added a term $d_3(\partial^3 a/\partial t^3)$ to Eq. (1). Here d_3 is a dimensionless third-order dispersion coefficient, which is normalized to $t_g{}^3$. To solve the resulting differential equation, we now make the ansatz

$$a(k, t) = a_0 \operatorname{sech}^{1+i\psi}[(t - \vartheta k)/t_p] \times \exp\{i[\phi k + \omega(t - \vartheta k)]\}, \quad (5)$$

where ϑ is the pulse delay after one full round trip (normalized to t_g) with respect to the local time frame and ω is the frequency detuning (normalized to $t_g{}^{-1}$) from the center frequency of the bandwidth-limiting element.[22] These two additional parameters become necessary for describing the effect of third-order dispersion. After inserting the ansatz (5) into the modified laser equation (1), we now obtain six iterative relations for the pulse parameters. The first three equations are composed of Eqs. (4a), (4b), and (4c) supplemented by the additional terms

$$-\omega(21d_3\psi + \vartheta\psi t_p{}^2) - d\psi\omega^2 t_p{}^2 - d_3\omega^3\psi t_p{}^2,$$

$$\omega[3\vartheta + \theta\psi^2 - (25 + 9\psi^2)d_3/t_p{}^2] - \omega^2(6d - 5\psi - d\psi^2 + \phi t_p{}^2 - \sigma a_0{}^2 t_p{}^2) - \omega^3(10d_3 - d_3\psi^2 + \vartheta t_p{}^2) - d\omega^4 t_p{}^2 - d_3\omega^5 t_p{}^2,$$

$$3d_3\omega\psi - \omega^2 t_p{}^2,$$

respectively. To the expression for the phase delay [Eq. (4d)] the term $\omega(3d_3\omega/t_p{}^2 - \vartheta) + d\omega^2 + d_3\omega^3$ has to be added. The two additional equations for the pulse delay per round trip, ϑ, and frequency detuning, ω, are

$$\vartheta = \frac{\omega(2 - 4d\psi + 2d^2\psi^2) + \omega^2 d_3(9d\psi^2 - \psi) + 9\omega^3 d_3{}^2\psi^2 - 8d_3\psi(\alpha - l + \sigma a_0{}^2)}{-\psi + d\psi^2 + 3d_3\omega\psi^2}, \quad (6)$$

$$\omega' = \omega + \frac{8d_3\psi - t_p{}^2(2\omega + \vartheta\psi - 2d\omega\psi - 3d_3\psi\omega^2)}{t_p{}^4}, \quad (7)$$

respectively. As is obvious from Eqs. (6) and (7), a nonzero third-order dispersion term gives rise to a pulse group delay (with respect to the local time) and a detuning of the carrier frequency from the center of the bandwidth-limiting element. Figures 8(a) and 8(b) show the chirp evolution and the frequency shift, respectively, plotted for the same parameters as used in Fig. 7(d) and with $d_3 = -30$. In Fig. 7(d) a stable pulse operation is periodically disturbed by an increase in the pulse amplitude. Figure 8 is a zoomed-in snapshot describing the chirp and the frequency shift during these bursts. Figure 9 shows in detail the evolution of the pulse spectrum near the peak of the *Q*-switched pulse envelope. The calculated time-dependent spectral features are in qualitative agreement with the experimental observations shown in Fig. 2.

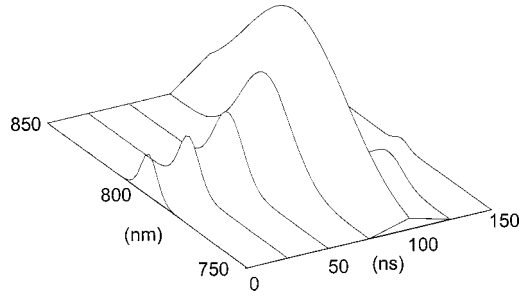

Fig. 9. Calculated pulse spectrum at different times near the peak of the *Q*-switched pulse for the parameters of Fig. 8.

4. CONCLUSIONS

Kerr-lens model-locked (KLM) Ti:sapphire lasers can be operated in regimes where periodic oscillations of the pulse amplitude on a time scale of several hundred kilohertz exist. Two such regimes were observed at intracavity group delay dispersion (GDD) larger or smaller than what is required for stable mode locking. Stabilization of the pulse amplitude modulation can be accomplished by weak modulation of the pump laser with a signal derived from the modulated Ti:sapphire pulse train. The nature of the self-modulation is similar to relaxation oscillations well known in solid-state lasers. A theoretical model of the femtosecond laser that takes into account gain saturation, dispersion, self-phase modulation, and Kerr lensing explains the trigger of the self-modulations by the interplay of nonlinear self-phase modulation and dispersion. In particular, the strong variation of the pulse spectrum observed during the oscillation spikes can be explained by the theory when third-order dispersion is included. Depending on the relative contribution of SPM and GDD, two different pulse stabilization mechanisms exist—the interaction of strongly chirped pulses with the bandwidth-limiting element and the Schrödinger-soliton stabilization mechanism for nearly chirp-free pulses.

ACKNOWLEDGMENTS

This study was supported in part by the W. M. Keck Foundation and the National Science Foundation (PHY-9601890). V. L. Kalashnikov, I. G. Poloyko, and D. O. Krimer acknowledge financial support from the Belorussian Foundation for Basic Research (F97-256). We thank both referees for the helpful suggestions and comments.

W. Rudolph, the corresponding author, can be reached at the address on the title page; by telephone, 505-277-2081; by fax, 505-277-1520; or by e-mail, wrudolph @unm.edu.

REFERENCES

1. E. W. Castner, J. J. Korpershoek, and D. A. Wiersma, "Experimental and theoretical analysis of linear femtosecond dye lasers," Opt. Commun. **78**, 90–99 (1990).
2. T. Tsang, "Observation of high-order solitons from a mode-locked Ti:sapphire laser," Opt. Lett. **18**, 293–295 (1993).
3. F. W. Wise, I. A. Walmsley, and C. L. Tang, "Simultaneous formation of solitons and dispersive waves in a femtosecond dye ring laser," Opt. Lett. **13**, 129–131 (1988).
4. V. Petrov, W. Rudolph, U. Stamm, and B. Wilhelmi, "Limits of ultrashort pulse generation in cw modelocked dye lasers," Phys. Rev. A **40**, 1474–1483 (1989).
5. Q. R. Xing, W. L. Zhang, and K. M. Yoo, "Self-*Q*-switched self-modelocked Ti:sapphire laser," Opt. Commun. **119**, 113–116 (1995).
6. A. Baltuska, Z. Wei, M. S. Pshenichnikov, D. A. Wiersma, and R. Szipöcs, "All solid-state cavity dumped sub-5-fs laser," Appl. Phys. B **65**, 175–188 (1997).
7. D. Cote and H. M. van Driel, "Period doubling of a femtosecond Ti:sapphire laser by total mode locking," Opt. Lett. **23**, 715–717 (1998).
8. S. R. Bolton, R. A. Jenks, C. N. Elkinton, and G. Sucha, "Pulse-resolved measurements of subharmonic oscillations in a Kerr-lens mode-locked Ti:sapphire laser," J. Opt. Soc. Am. B **16**, 339–344 (1999).
9. J. C. Diels and W. Rudolph, *Ultrashort Laser Pulse Phenomena* (Academic, San Diego, Calif., 1996).
10. H. Haus, "Theory of mode locking with a fast saturable absorber," J. Appl. Phys. **46**, 3049–3058 (1975).
11. D. Kühlke, W. Rudolph, and B. Wilhelmi, "Calculation of the colliding pulse mode-locking in CW dye ring lasers," IEEE J. Quantum Electron. **QE-19**, 526–533 (1983).
12. H. A. Haus, J. G. Fujimoto, and E. P. Ippen, "Analytic theory of additive pulse and Kerr lens mode locking," IEEE J. Quantum Electron. **28**, 2086–2096 (1992).
13. T. Brabec, Ch. Spielmann, P. F. Curley, and F. Krausz, "Kerr lens mode locking," Opt. Lett. **17**, 1292–1294 (1992).
14. J. L. A. Chilla and O. E. Martinez, "Spatial-temporal analysis of the self-mode-locked Ti:sapphire laser," J. Opt. Soc. Am. B **10**, 638–643 (1993).
15. V. Magni, G. Cerullo, S. de Silvestri, and A. Monguzzi, "Astigmatism in Gaussian-beam self-focusing and in resonators for Kerr-lens mode locking," J. Opt. Soc. Am. B **12**, 476–485 (1995).
16. V. P. Kalosha, M. Müller, J. Herrmann, and G. Gatz, "Spatiotemporal model of femtosecond pulse generation in Kerr-lens mode-locked solid-state lasers," J. Opt. Soc. Am. B **15**, 535–550 (1998).
17. V. L. Kalashnikov, I. G. Poloyko, V. P. Mikhailov, and D. von der Linde, "Regular, quasi-periodic, and chaotic behavior in continuous-wave solid-state Kerr-lens mode-locked lasers," J. Opt. Soc. Am. B **14**, 2691–2695 (1997).
18. V. L. Kalashnikov, V. P. Kalosha, I. G. Poloyko, V. P. Mikhailov, M. I. Demchuk, I. G. Koltchanov, and H. J. Eichler, "Frequency-shift locking of continuous-wave solid-state lasers," J. Opt. Soc. Am. B **12**, 2078–2082 (1995).
19. F. X. Kärtner, I. D. Jung, and U. Keller, "Soliton mode locking with saturable absorbers: theory and experiments," IEEE J. Sel. Top. Quantum Electron. **2**, 540–556 (1996).
20. J. Herrmann, "Theory of Kerr-lens mode locking: role of self-focusing and radially varying gain," J. Opt. Soc. Am. B **11**, 498–512 (1994).
21. A. M. Sergeev, E. V. Vanin, and F. W. Wise, "Stability of passively modelocked lasers with fast saturable absorbers," Opt. Commun. **140**, 61–64 (1997).
22. V. L. Kalashnikov, V. P. Kalosha, I. G. Poloyko, and V. P. Mikhailov, "New principle of formation of ultrashort pulses in solid-state lasers with self-phase-modulation and gain saturation," Quantum Electron. **26**, 236–242 (1996).